Egypt. J. Chem. **Vol. 64,** No. 3 pp. 1293 - 1313 (2021)

Egyptian Journal of Chemistry

http://ejchem.journals.ekb.eg/

Sugarcane Bagasse Biochar with Nanomagnetite: A novel Composite Heavy Metals Pollutants Removal

Ola M. Abd Almawgood[a], Sayed A. El Tohamy[a], Eman H. Ismail[b], Farag A. Samhan[c*]

[a] *Environmental Research Department, Land, Water and Environment Institute, Agricultural Research Center (ARC), Ministry of Agriculture and Land Reclamation, 9-Cairo university street, Giza, 12112, Egypt*

[b] *Chemistry Department, Faculty of Science, Ain Shams University, Abbassia, 11566, Cairo, Egypt*

[c] *Water Pollution Research Department, National Research Center, Dokii, 12662, Giza, Egypt*

Abstract

In this novel, we developed a modern and efficient adsorbent that may serve as environmental protection and sustainable development for removing some metal ions such as Fe and Zn from aqueous solution. The new adsorbent was synthesized by mixing the sugarcane bassage biochar with nano-magnetite (SCB-BC/Fe_3O_4) to form nano-composite. High resolution transmission electron microscope (TEM) imaging shows the synthesized nano-composite with 40 nm average diameters. The adsorption kinetic of metals on the nano-composite was discussed, and the equilibrium equation of the metal ions was found following Langmuir isotherm model. The experimental data showed that the synthesized (SCB-BC/Fe_3O_4) nano-composite can quantitatively remove the metal ions from water by removal efficiencies of 90% and 96% for Fe and Zn respectively. It can be concluded that the synthesized adsorbent can be used for removal of heavy metals from water and/or wastewater as one of the treatment stages in treatment plants.

Keywords: Nano-materials**,** Nano-composites**,** Wastewater treatment

1. Introduction

Our current water supply is facing huge challenges. To date, statistics by WHO (2012 and 2014) has shown that nearly half of the world population will suffer from water scarcity in 2025 [1]. Heavy metals dispersed in the environment are badly affecting human health [2]. Mining, smelting, fertilizer and pesticide application, and electronic output discharge have increased the danger associated with heavy metals discharged into the aquatic environment contributing to metal water pollution [3]. Studies have shown that wastewater constituting high spectrum of heavy metals which produced from heavy industries like battery, vehicle and steel manufactories [4]. Metal ions are transmitted to the body by food or water consumption and cause serious health damage water [5]. Many heavy metals are highly toxic to humans, even at low levels [6]. Adsorption, selective separation, ion-exchange, reverse osmosis, filtration, bioremediation, supercritical fluid extractions are techniques have been used to remove metal ions from water [5]. But, adsorption is considered to be one of the most promising techniques, especially for effluents of low concentrations of these pollutants [7]. Biochar is a low-cost absorber to remove various types of pollutants [8], derived from agricultural wastes have taken greatca re to remove heavy metals from wastewater [9]. Higher content and difficult biodegradable carbon of the biochar are distinguishing character, besides containing some nutritive hydrocarbons [10].The sugarcane bagasse biomass has been used in this study as a biochar source the plant has three main sections: the green tops, the stem and the roots. For sugar production the stem or stalk is milled and crushed at the front end of the mill where the sugarcane juice is extracted, the remaining dry fibrous residue is called sugarcane bagasse [11], although the biochar production from plant residues is not costly, it still has limited effect

*Corresponding author e-mail: faragsamhan@gmail.com.
Receive Date: 16 September 2020, Revise Date: 12 December 2020, Accept Date: 21 December 2020
DOI: 10.21608/EJCHEM.2020.43158.2870

in metal ions removal, so we suggested to mix with effective nano-material increasing its reactivity.Metal oxide nanoparticles are commonly used, Higher energy consumption and unsafe techniques mostly used to produce metal oxide nanomaterials, taken as one of the advantages prioritizing biochar as promising material [12]. In addition to the achievements in technical activates facilitating production of magnetic nanostructures as magnetite (Fe_3O_4) and maghemite, (γ-Fe_2O_3) [13]. The nano-metal oxides differentiated with large surface area associated with super-paramagnetic properties, and short interregional-particle diffusion range, more adsorption categories, compacted without massive decrease of surface area, and the easily reusing of these materials [14]. Its isolation can become a real challenge by using nano-materials in the water treatment system. Generally, the main disadvantage of nanoparticles is the cost of production, regeneration and recovery is also a difficult process, as the nanoparticles used can subsequently become a type of environmental pollution. Therefore, new adsorbents with high specific surface area and low operating costs need to be identified [15].Nano-composite technology has been shown to be an effective and promising solution. Through mounting desired nanoparticles on different supporting materials, such as polymers or membranes, nano-composite is commonly manufactured. Nano-composites are multiphase material with constituent assembly 100 nm at least, that showed economic effectiveness, renwable and highly efficient [1]. The nano-metal supported biochar could resolve the significant limitations of the biochar and increase its effectiveness in heavy metals removal [16]. The magnetite-based biochar, that contains rough surface and high attractive sites is becoming widely known in the heavy metals removal [17].In the present study, we aimed to produce an economic, sustainable, good mechanical and chemical resistance, handleably and regeneratable biochar from agricultural residue (sugarcane bagasse) as a sustainable adsorbent. The adsorbent can be used after mixing with nanomaterial like iorn oxide (nano-magnetite) in a composite for removing higher concentrations of Fe, Zn and microorganisms. The new composite was used in real wastewater samples collected from the final effluent of a municipal wastewater treatment plant (Fayuom city, Quhafa, ezbet Henin). Iron oxide (magnetite) nanostructures were produced by co-precipitation of the iron salts, base and the biochar produced by slow pyrolysis at 300ºC for 1h. The composite was characterized by means of different techniques then used as adsorbent for batch experiments then applied on the real wastewater samples. The real samples were controlled, preserved and examined according to "Standard Methods for the Examination of Water and Wastewater" American Public Health Association [18].

2. Experimental

2.1 Materials

2.1.1 Magnetite production

Magnetic iorn oxide (magnetite) nanoparticles suspension was synthesized using co-precipitation method by dissolving ferric chloride $FeCl_3$. $6H_2O$ and ammonium ferrous sulphate ($(NH_4)_2Fe\ (SO_4)_2$) using NaOH as a base. All the chemicals used in analytical grade supplied by Sigma-Aldrich Company and exploited without further purification**.**

2.1.2 Biochar production

Biochars used throughout this research were derived from sugarcane bagasse collected from Fayoum governorate. The feedstock has been dried for 24 h at 103 °C in an oven (Fisher Scientific, U.S.A). Pyrolysis was performed in limited oxygen in order to maintain an oxygen free atmosphere at two temperatures degree 300 °C and 600 °C in a muffle furnace (Barnstead, Thermolyne, U.S.A). The rate of temperature increase was 20°C /minute. Sample was retained in the operating furnace for 60 min after reaching the targeted temperature. Biochar was subsequently removed and cooled in desiccator, weighted and tightly sealed plastic containers. To select the workable biochar, we applied the two biochars produced to 1 ppm of each standard (Fe and Zn) and recorded the removal efficiencies (Table 1).

Table 1: Removal efficiencies of SCB-BC burned at 300 °C and at 600 °C for 1ppm Fe and 1ppm Zn

Biochar temp.	Fe Conc ppm	Fe R %	Zn Conc ppm	Zn R %
SCB-BC at 300 °C	0.511	48.90	0.668	33.20
SCB-BC at 600 °C	0.673	32.70	0.690	31.00

2.2 Methods

2.2.1 Preparation of biochar- iorn oxide (SCB-BC/ Fe_3O_4) composite

The biochar/nanomagnetite nanocomposites prepared by physical mixing of ratios from the powder samples. Different ratios were mixed physically from Fe_3O_4 and SCB-BC with percent weights 0.0, 0.1, 0.2, 0.5, 0.6, 0.8, and 1.0 (Table 2) [19].

2.2.2 Selection the SCB-BC/Fe_3O_4 nanocomposites effective ratio

Two stock solutions 1000mg/l (Fe) and (Zn) separately as Fe $(NO_3)_3$ (Fe in HNO_3) and Zn $(NO_3)_2$ (Zn in HNO_3) were used. Working solutions were prepared after diluting the stocks to 1ppm of both Fe and Zn. Different ratios of **(SCB-BC / Fe_3O_4)**

composite were used separately as shown in (Table 2). Dose of 1g/L [20] from each was applied to the two working solutions. The experiments were done by mixing (0.15 g) of each composite ratio with (150 mL) of (1 mg/l) Fe, Zn) separately as a working solution, then the samples agitating on an orbital shaker SK-600, korea (serial no; M059119) at (200 rpm) [20] for (15 min) at room temperature. The contact time had been determined by kinetic experiments. ***Once the reactions ended***, samples were removed and filtered (Whatman GF/C) for removing debris and measuring the residues of metal contents using ICP-OES (Parkin Elmer, Optima 5300 DV, Serial No: 077C&0220701). The difference between the start and final metal content represent the removed concentration.

$C_{ads}=C_i(1mg/l)-C_f$ → (1)

Where;

C_{ads}; adsorbed metal ion concentrations mg/l

C_i; initial metal ions concentrations (=1mg/l)

C_f; final aqueous concentration of metal ions mg/l

The efficiency of the composite ratios in metal ions removal was calculated according to the following equation;

Removal efficiency (%)= $[(C_i-C_f)/C_i]X100$ → (2)

Where;

C_i ; initial concentrations of metal ions (=1mg/l)

C_f; final concentrations of metal ions mg/l

Table 2: Preparation of novel SCB-BC/Fe_3O_4 nanocomposite of homogeneous form

X ratios	Fe_3O_4 (1-x)	SCB-BC (x)	SCB-BC (x) wt.%	Fe_3O_4 (1-x) wt.%
1	0	1	100	0
0.9	0.1	0.9	90	10
0.8	0.2	0.8	80	20
0.5	0.5	0.5	50	50
0.4	0.6	0.4	40	60
0.2	0.8	0.2	20	80
0	1	0	0	100

2.2.3 Characterization

The morphology of SCB-BC at 300 °C and SCB-BC/ Fe_3O_4 nano-composite was examined by high-resolution transmission electron microscope (HR-TEM) (JEOL 1200 EXll, JAPAN). Using a Fourier transform infrared spectrometer (FTIR) (JASCO-IR) the surface structural groups of SCB-BC /Fe_3O_4 composite were characterized before and after adsorption, with scanning range from 4000 to 400cm^{-1}. The spectra were collected with a resolution of 0.964233 cm^{-1} transmittance. The particle size distribution of SCB-BC/ Fe_3O_4 composite was measured by a laser particle size analyzer (Malvern, ra200:200 mV).

2.2.4 Kinetic experiments

The kinetic experiment was carried out using 1000 mg/L of Fe and Zn, separately. The experiment was done by mixing a fixed dose (0.15g) each the effective composite ratio (50% SCB-BC: 50% Fe_3O_4) with (150 mL) working solution of (1 mg/l) from Fe and Zn separately. Samples were stirred at room temperature on an orbital shaker (200 rpm) time intervals 15min-120 min) (Table 4). By the end of each interval, samples were filtered (Whatman GF/C filters). Metal content were assessed in the supernatants **(ICP-OES)**. The adsorbed metal concentrations were calculated from equation (1) and the removal efficiency of the composite was calculated from equation (2).

2.2.5 Equilibrium experiment

The equilibrium experiment was done using 1000 mg/L (Fe) and 1000 mg/L (Zn), separately. The experiment was done by mixing a fixed dose (0.15g) of the effective composites ratio (50% SCB-BC: 50% Fe_3O_4) with (150mL) working solution of varying concentrations (1-10mg/l) from Fe and Zn separately (Table 5), the samples then agitated on an orbital shaker at (200rpm) for (15min) at room temperature. By the end of each interval, samples were filtered (Whatman GF/C filters). Metal content were assessed in the supernatants **(ICP-OES)**. The adsorbed metal concentrations were calculated from equation (1) and the removal efficiency of the two composites was calculated from equation (2).

2.2.6 Application of SCB-BC/Fe_3O_4 nanocomposite on the real samples of the effluent collected from the domestic wastewater treatment plant

(0.15 g) of the effective composite ratio (50% SCB-BC: 50% Fe_3O_4) was applied to 150mL working solution of the plant effluent samples as a real sample by the batch technique as equilibrium and kinetic experiments. The samples were analyzed chemically and microbiologically before and after adsorption according to [18] then the adsorbed pollutants concentrations were calculated from equation (1), and the removal efficiency of the two composites was calculated from equation (2).

Table 3: Removal efficacy of SCB-BC/Fe_3O_4 nanocomposite for 1ppm solutions of each Fe and Zn solutions

X ratios of SCB-BC	Adsorbed Fe Concs. ppm	R% of Fe	Adsorbed Zn Concs. ppm	R% of Zn
(100% SCB-BC) 1g SCB-BC\0g Fe_3O_4	0.511	48.9%	0.668	33.2%
(90% SCB-BC) 0.9g SCB-BC\0.1g Fe_3O_4	0.426	57.4%	0.627	37.3%
(80% SCB-BC) 0.8g SCB-BC\0.2g Fe_3O_4	0.42	58.0%	0.623	38.0%
(50% SCB-BC) 0.5g SCB-BC\0.5g Fe_3O_4	0.096	90.0%	0.04	96.0%
(40% SCB-BC) 0.4g SCB-BC\0.6g Fe_3O_4	0.048	95.2%	0.071	92.9%
(20% SCB-BC) 0.2g SCB-BC\0.8g Fe_3O_4	0.327	67.3%	0.008	99.2%
(0% SCB-BC) 0g SCB-BC\1g Fe_3O_4	0.766	23.4%	0.023	97.7%

Table 4: Time intervals for kinetic experiment for 1ppm of Fe and Zn mixed by 50%:50% working ratios of SCB-BC/Fe_3O_4 nanocomposite

Time (min)	Adsorbed Fe Concs. ppm	Average	R% of Fe on SCB-BC/ Fe3O4	Adsorbed Zn Concs. ppm	Average	R% of Zn on SCB-BC/ Fe3O4
5	0.388	0.388	61.20%	0.06	0.07	93.00%
	0.638			0.08		
10	0.258	0.258	74.10%	0.04	0.045	95.50%
	0.688			0.05		
15	0.105	0.096	90.00%	0.04	0.04	96%
	0.096			0.14		
30	0.165	0.165	83.50%	0.0425	0.0425	95.80%
	0.53			0.1		
45	0.178	0.178	82.20%	0.04	0.045	95.50%
	0.768			0.05		
60	0.176	0.1765	82.40%	0.09	0.02	98.00%
	0.462			0.02		
120	0.108	0.175	82.50%	0.01	0.02	98.00%
	0.175			0.02		

Table 5: Equilibrium experiment for different concentrations of Fe and Zn (ppm) mixed by 50%:50% working ratio of SCB-BC/Fe_3O_4 nanocomposite

Conc. (ppm)	Adsorbed Fe Concs. ppm	R % of Fe on SCB-BC/Fe_3O_4	Adsorbed Zn Concs. ppm	R% of Zn SCB-BC/Fe_3O_4
1	0.096	90%	0.03	97.0%
2	0.402	80%	1.154	42%
3	0.974	68%	2.254	25%
4	1.890	53%	3.403	15%
5	3.653	27%	4.653	7%
6	4.625	23%	5.715	5%
7	5.616	20%	6.792	3%
8	6.816	15%	7.8	3%
9	7.872	13%	8.817	2%
10	8.985	10%	9.83	2%

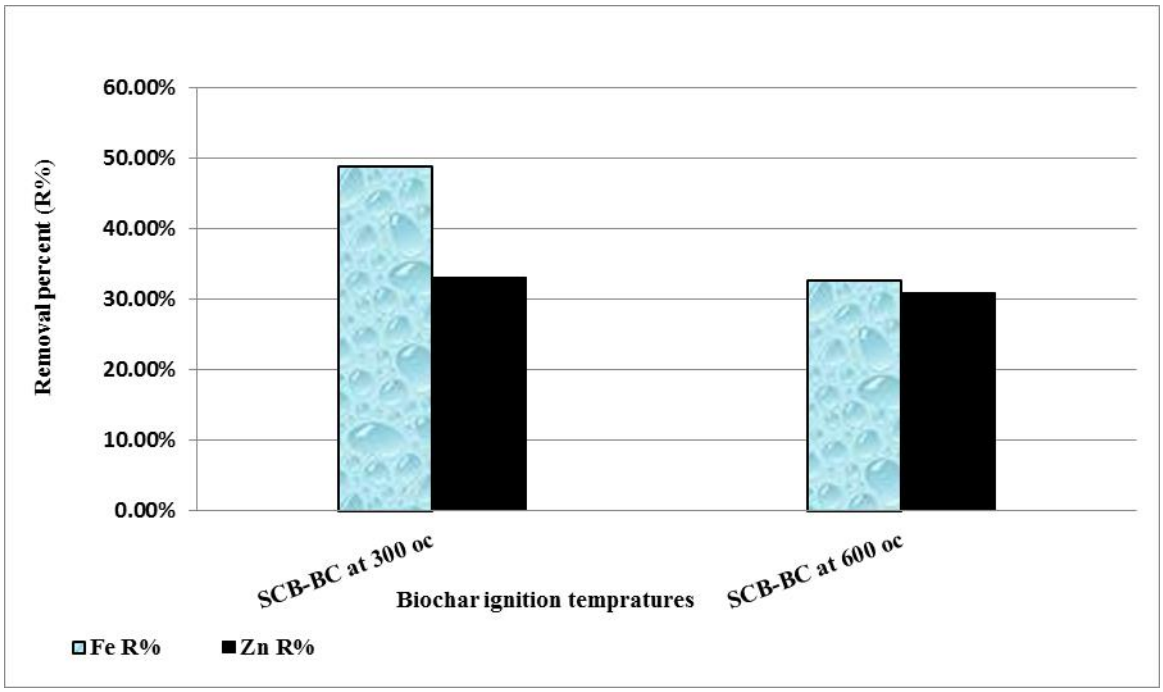

Fig. 1. Removal efficacy of Fe and Zn (1ppm) by SCB-BC burned at 300 ˚C and at 600 ˚C

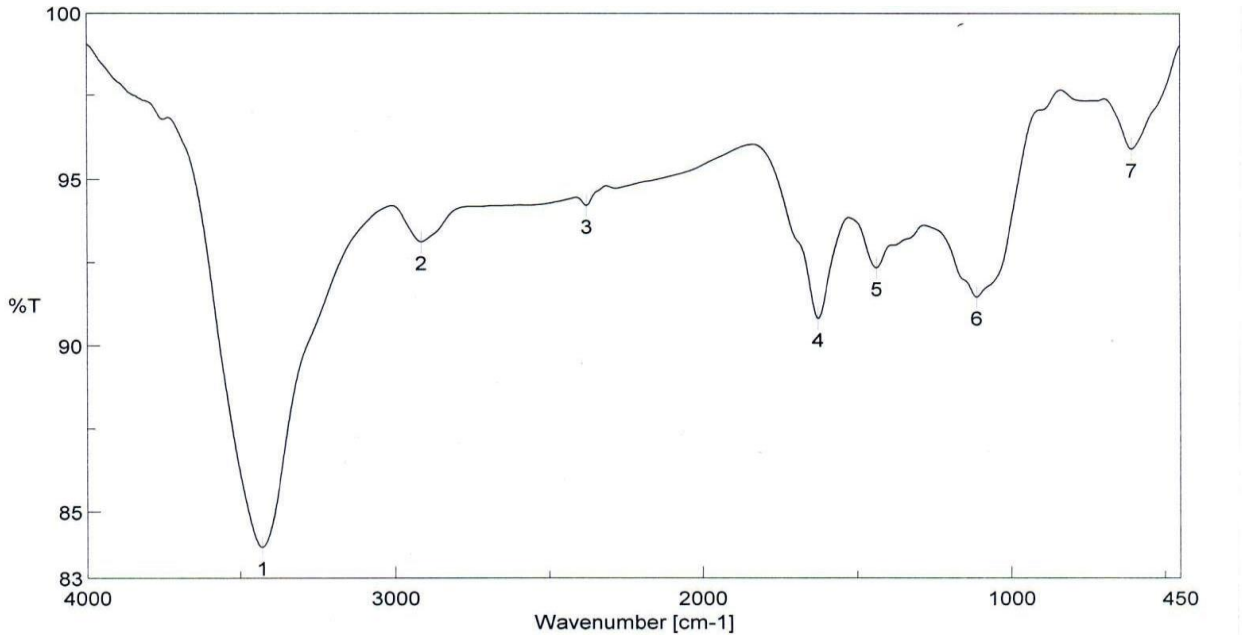

Fig. 2. FT-IR spectra of sugarcane bagasse biochar (SCB-BC) burned at 300 °C

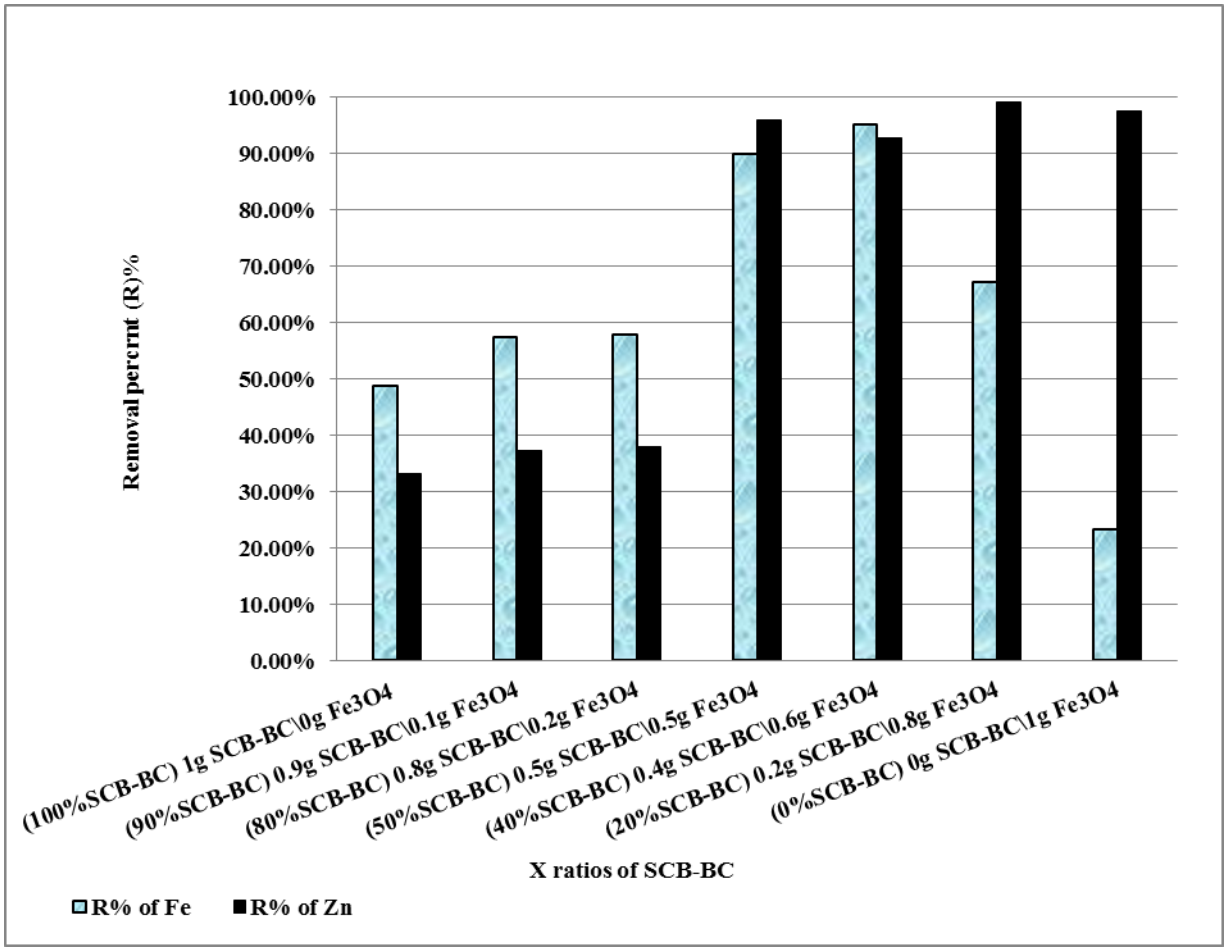

Fig. 3. (1ppm Fe and 1ppm Zn) removal by SCB-BC/Fe_3O_4 nanocomposite

3. Results and discussion

3.1 Selection of sugarcane bassage biocharpyrolysis temperature (SCB-BC) that will be mixed with nano-magnetite in the composite production

As mentioned in the methods, the SCB-biochar produced at two different temperatures (300 °C and 600 °C), so the effective biochar with acceptable iron and zinc removal efficiency should be selected. Table (1) and fig.(1) showed that the SCB burned at 300 °C produced biochar with higher removal efficacy for both iron and zinc (48.90% and 33.20% respectively) while the removal efficacies decreased to (32.70% and 31.00%) for both iron and zinc respectively when those ions were adsorbed on the SCB-biochar produced at 600 °C. This may be related to the oxygen content of functional groups that have positive effects on adsorption potential, while these groups may be declined at higher temperature. These phenomena discussed by [21] that related the removal efficiencies decreases at higher temperature to the following; on pyrolysis cellulose transformed to a porous cellulosic precursor, it was converted into an irregular carbohydrate then to aromatic carbons as end products. Decarboxylation, dehydrogenation, dehydration, de-oxygenation, and aromatization were the reactions occurred during the cellulose pyrolysis, the dehydration reaction results in breakdown of the hydrogen bonds indicating the primary process occurred at temperature 300 °C this confirmed by appearance of the strong beak no (1) at 3429 cm^{-1} (O-H) stretching vibration attributed to alcohols, phenols breakdown of (H-bonding) on the FTIR spectrum in our study fig (2). On the other hand, the hemicellulose component is converted into porous smooth material with further increasing in the temperature, previous reactions reduced hydroxide ions and carboxyl groups decreasing the adsorption capcity. As a result to the previous discussion we used the SCB-BC produced at 300 °C in mixing with nano-magnetite to form nano-composite for iron and zinc removal.

3.2 Selection the SCB-BC/Fe_3O_4 nano-composites effective ratio

Tables (2,3) and fig. (3) Showed the removal efficiency of 1ppm of both Fe and Zn using different ratios of SCB-BC/Fe_3O_4 nano-composite. The removal efficiencies of Fe and Zn ions reached (48.9% and 33.2%) respectively when the SCB-biochar used individually, this noted in the ratio 100 % SCB-BC (1g SCB-BC\0g Fe_3O_4) as the removal of the metal ions in here depended on the functional groups founded on the biochar surface. As being said, the raw biochars that directly produced from feedstocks usually have restricted functional surface groups and relatively low surface area with limited porous structure due to the perceived properties of lignocellulosic constituents and moderate temperature of pyrolysis. And as a result of the limited active sites, fresh BC has lower metal ion removal efficiencies than other identified adsorbents [16]. On the other hand, mixing the magnetite nano-particles (Fe_3O_4) with the as prepared SCB-biochar increases the removal efficiencies of both Fe and Zn ions gradually. This was noted by addition of different doses of the magnetite nano-particles (Fe_3O_4), as noted for the ratio of 90 % SCB-BC (0.9g SCB-BC\0.1g Fe_3O_4) the removal efficiencies for both Fe and Zn ions were (57.4% and 37.3%) respectively, and for the ratio of 80 % SCB-BC (0.8g SCB-BC\0.2g Fe_3O_4) the removal efficiencies for both Fe and Zn ions were (58% and 38%) respectively. i.e. the surface properties of the nano-magnetite improved the adsorption capacity of the SCB-biochar. Nanometals-aided biochar have been used in removal of toxic metals from sewage water. Loading of nano-metals on the surface or on the pores of biochar changed its physicochemical characteristics such as variance in surface porosity, graphite shape formation, and surface load and surface functional group shift [16]. For the ratio of 50 % SCB-BC (0.5g SCB-BC\0.5g Fe_3O_4) we noted acceptable removal efficiencies for both Fe and Zn ions (90% and 96%) respectively. The increase in the removal efficiencies that has been achieved by increasing the dose of the nano-magnetite added to the SCB-biochar may be related to the increase in the number of the –OH groups on the nano-magnetite surface resulted from the NaOH and the starch molecules used in preparation of nano-magnetite by co-precipitation, also Fe-O on the magnetite surface may helped in the metal ions removal. As discussed by [16], the surface oxides or hydroxides were demonstrated towards the metal ions improving complexes formation by liquid coordinative bonds between metal-ligand transferring metal ions to H-Fe-O-$\{M\}^{n+}$ species. The higher removal of Fe ions (95.2%) appeared at 40% SCB-BC (0.4g SCB-BC\0.6g Fe_3O_4) may be related to the increased surface functional groups and surface charge added to the composite by increasing the magnetite concentration, indicating that ion exchange and electrostatic interactions may have occurred between these groups and Fe ions. These mild electrostatic interactions were due to the hydrolysis of OH groups increasing the negative charge on the composite surface attracting much Fe ions (i.e the adsorption efficiency increased). The higher removal of Zn ions (99.2%) appeared at 20% SCB-BC (0.2 g SCB-BC\0.8 g Fe_3O_4) also may be related to increase the magnetite concentration in the composite surface producing more Fe-O molecules attracting much Zn ions forming H-Fe-O-Zn complexes or by the OH groups forming Zn-O as this is the key method for removing the Zn^{2+} metal ions as mentioned by [22]. Finally, Fe removal efficiency noted to be decreased of by further increase of nano-magnetite dose to reach its minimum value (23.4%) at (100% Fe_3O_4) 0g SCB-BC\1g Fe_3O_4, this may be related to suber-saturation. As mentioned by [23] because of their high reduction reactivity serving as electron donors, the iron oxides nano-particles have attached much attention, the Fe^{2+} ions in the core-shell structure of Fe_3O_4 nano-particles can effectively reduce Fe^{3+} ions of the standard to Fe^{2+} completing the magnetite reaction in the solution. In addition, certain surface functional groups, such as C-H or C-OH, have certain reduction reactivity. Many oxidizing agents in the solution can easily oxidize Fe^{2+} ions to Fe^{3+}. Thus [24] used magnetite as a stationary surface sorbent to remove Fe ions from aqueous solutions. The analysis indicated that Fe metal ions (Fe^{2+} and Fe^{3+}) adsorbed on magnetite with the same affinity. Fe^{2+} and Fe^{3+} content can be separated from water by the suggested approach and the composite can't differentiate considerably between these ions. For the Zn removal it was also noted small decrease of its removal efficiencies by further increase of nano-magnetite dose (97.7%) at (100% Fe_3O_4) 0g SCB-BC\1g Fe_3O_4, this may be related to suber-saturation as the composite pores completely occupied by Zn ions. Nano-crystals present on the composite surface can discharge metal ions that may form porous ion depositions [16]. The formed precipitation is stable and appears to be established, reducing the mobility of metal ions. According to these phenomena, after the super-saturation of the composite by the adsorbed Zn further concentrations of Zn would transfer to ZnO and Zn-Fe precipitation. Finally, from the above results we selected the ratio of 50% SCB-BC: 50% Fe_3O_4 (0.5g SCB-BC\0.5g Fe_3O_4) as a working ratio for the pollutants removal is it the most economic ratio.

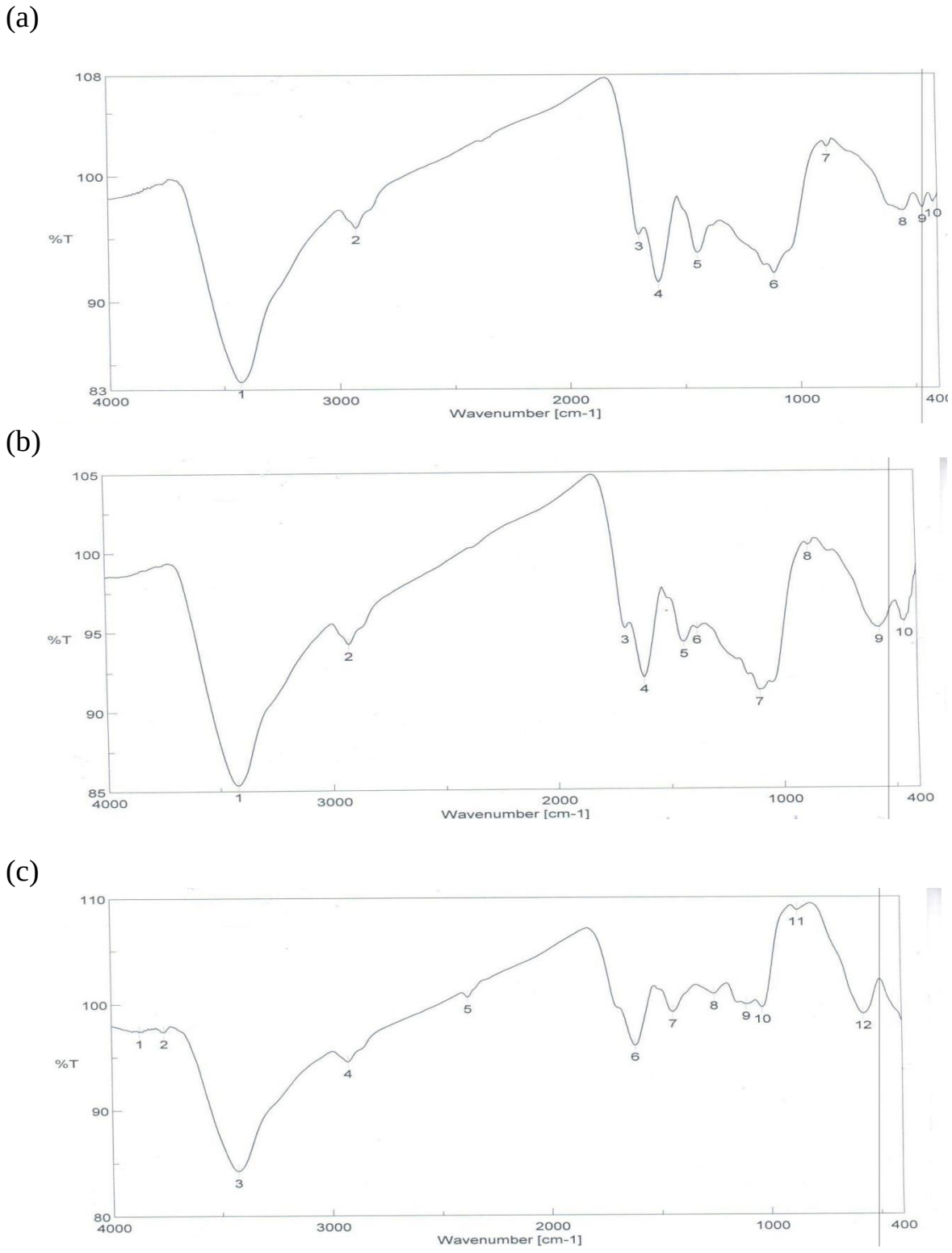

Fig. 4. FT-IR spectra of SCB-BC/Fe_3O_4 nano-composite, before and after (Fe and Zn) adsorption, (a) pure composite, (b) adsorption of Fe on the composite and, (c) adsorption of Zn on the composite

3.3 Characterization of (SCB-BC/Fe_3O_4) nano-composite

3.3.1 FTIR Spectra

Fig. (2), shows the FTIR spectrum of sugarcane bassage biochar burned at 300 °C. The spectrum showed different peaks indicating the existence of polysaccharides and polyphenolics [25]. The strong beak no (1) at 3429 cm^{-1} (O-H) stretching vibration attributed to alcohols, phenols (H-bonding) and polymeric compounds indicating the presence of cellulose, hemi-cellulose and lignin in the bagasse skeleton [26, 27, 28]. Peak no (2) at 2914 cm^{-1} (-CH) attributed to stretching for alkyl group (-CH_3 and -CH_2 groups) [26, 27, 28], these two peaks agreed with [29, 30] FTIR Spectrum of sugarcan bagasse biochar (SCB-BC). Peak no (3) at 2377 cm^{-1} attributed to (O-H) overlaps C-H stretching of adsorbed water in the lattice matrices. Peaks no (4) at 1626 cm^{-1} this peak may be related to (C=C) stretching vibration of dis-substituted alkene and may be related to a conjugated (C=O) this peak agreed with [31] FTIR Spectrum of sugarcane bagasse biochar (SCB-BC). Peak no (5) at 1437 cm^{-1} (C-O) stretching attributed to carboxylic groups indicating that carboxylic acids were included in the lignin and hemi-cellulose of the sugarcane bagasse skeleton proving that the sugarcane bassage is an organic compound, this peak agreed with [30] FTIR Spectrum of sugarcane bagasse biochar (SCB-BC). Peak no (6) at 1112 cm^{-1} attributed to (C-O) stretching vibration might be due to alcohols [32] and broad peak no (7) at 607 cm^{-1} attributed to (≡C-H) indicate bending alkyne skeleton describing the extent of polymerization of the biochar. The data of the FTIR spectrum indicated that the bagasse skeleton free from nitrogen and sulfur groups and this agreed with [30, 33] sugarcane bagasse biochar (SCB-BC) spectrum. It was therefore found from FTIR spectra data that sugarcane bagasse biochar consists of groups of hydroxyl and carboxylate. These functional groups reflect the hydrophilic nature and can serve as anchoring sites for ferrite particles in nanomagnetite when mixed with this biochar in the preparation of (SCB-BC/ Fe_3O_4) nanocomposite [26].

Fig. (4a), shows the FTIR spectrum of (SCB-BC/ Fe_3O_4) nano-composite that formed by mixing of sugarcane biochar with nano-magnetite. Comparing this spectrum with SCB-BC spectrum fig. (2), there are two common characteristic peaks for sugarcane biochar with stable appearance, peak no (1) at 3429 cm^{-1} attributed to (O-H) groups of alcoholic and phenolic skeleton, and peak no (6) at 1112 cm^{-1} (C-O) stretching vibration might be due to alcohols. It is noted some changes in the spectrum marked as follow;

1- The peak no (2) represent small shift of (-CH) stretching for alkyl groups (-CH_3 and -CH_2 groups) from 2914 cm^{-1} to 2924 cm^{-1}, peak no (4) represent small shift of (C-O) asymmetric from 1626 cm^{-1} to 1613 cm^{-1}, and peak no (5) represent small shift of (C=O) stretching vibration from 1437 cm^{-1} to 1444 cm^{-1}, these small shifts indicated reaction of functional groups on sugarcane bagasse biochar with nano-magnetite.

2- Disappearance of peak no (3) at 2377 cm^{-1} of (-OH) groups from SCB-BC spectrum fig. (2) replaced by appearance of peak no (3) at 1696 cm^{-1} (C=O) attributed to carboxylic acid stretching, appearance of this peak agreed to FTIR Spectrum of [30] for sugarcane bagasse biochar (SCB-BC).

After the iron oxide transformation on to the surface of SCB-BC adsorbent, the FTIR spectra demonstrated significant changes which tend to make more crystallinity than in the sugarcane bagasse biochar (SCB-BC).

3- Appearance of new peak no (7) at 877 cm^{-1} attributed to (Fe-OH) stretching vibration [19] proving that iron of magnetite reacted with the alcoholic or phenolic (-OH) groups present in SCB-BC skeleton proving that it had successfully impregnated onto cellulose.

4- Appearance of new peaks no (8, 9) at 549 cm^{-1}, 464 cm^{-1}, related to (Fe-O) appearence [31, 34]. The peak at 464 cm^{-1} indicate a metal –oxygen bond proving that (C-O) carbonyl group present in SCB-BC skeleton worked as capping material forming layer around the magnetite nanoparticles, mentioned that the iron oxide impregnated on the biochar surface and the peak at 549 cm^{-1} prove that the C–C skeleton vibrations and C–H (substituted alkene) are presented [35].

Finally peak no (10) at 413 cm^{-1} attributed to octahedral and tetrahedral (Fe-O) of magnetite core [36]. The peaks no (7, 8, 9, and 10) proved that SCB-BC and magnetite interacted successfully forming composite. There were –OH and –COOH functional groups on the SCB-BC surface aided to bind the iron oxide particles, and then stuck to the char [27]. The intermolecular interaction may be strengthened with adhesion forces of hydrogen bonding phases between Fe–OH of the metal oxide and C–OH on the char surfaces, besides electrostatic interactions may take place. These electric interactions may tie the magnetite particles to the biochar molecules [27].

Fig. (4b) shows the FTIR spectrum of (SCB-BC/ Fe_3O_4) nano-composite after adsorption of Fe ions from the standard iron solution on its surface. Comparing with the FTIR spectrum of pure composite (fig. 3a) there were five common characteristic peaks with stable appearance, peak no (1) at 3423 cm^{-1} attributed to (OH) groups, peak no (2) at 2923 cm^{-1} (-CH) attributed to stretching for alkyl group, peak no (3) at 1695 cm^{-1} attributed to (C=O) carboxylic acid stretch, peak no (4) attributed to 1613 cm^{-1} (C-O) asymmetric, and peak no (8) at

878 cm^{-1} attributed to (Fe-OH) stretching vibration. The observed changes were as follow:

1- Peak no (5) represent small shift of (C=O) group from 1444 cm^{-1} to 1435 cm^{-1}.

2- New appearance of peak no (6) at 1375 cm^{-1} attributed to (C-H) deformation bending alkane (methyl group), appearance of this peak agreed to FTIR Spectrum of [30] for sugarcane bagasse biochar (SCB-BC). Also we can consider appearance of this peak at 1375 cm^{-1} is a large shift to carbonyl group at 1444 cm^{-1} and 1435 cm^{-1} proving that ion exchange might occurred between carbonyl group present on the composite surface and Fe^{3+} metal ion from the standard iron solution forming Fe-carbonate (i.e. the iron ions adsorbed on the composite surface), this exception agreed with [16] who noted the same shift for this peak after adsorption of Pb^{2+} and Cd^{2+} on iron oxide nanoparticles assisted biochar.

3- The peak no (7) represent small shift of alcoholic (C-O) group from 1112 cm^{-1} to 1104 cm^{-1}, this shift proves the reaction of this group present on the composite surface attracting the Fe^{3+} metal ion from the standard iron solution forming (Fe-O) (i.e. the iron ions adsorbed on the composite surface). This exception noted by shifting of the (Fe-O) peak from 549 cm^{-1} to peak no (9) at 567 cm^{-1} that related to vibrations of Fe^{2+} -O^{2-} (Fe-O) in tetrahedral sites [19].

4- Finally, disappearance of peak no (10) at 413 cm^{-1} of the octahedral and tetrahedral (Fe-O) of the magnetite core from the composite spectrum (fig. 3a), indicating that the Fe^{3+} metal ion from the standard iron solution might be reduced to Fe^{2+} that reacted with O from C=O forming Fe_2O_3, this reaction expected as result to appearance peak no (9) at 567 cm^{-1} that may be related to presence of hematite confirmed by shift of (Fe-O) peak at 464 cm^{-1} to peak no (10) at 456 cm^{-1} that related to vibrations of Fe^{3+} -O^{2-} (Fe_2O_3) in octahedral sites [19]. The reduction of Fe^{3+} ions to Fe^{2+} ions related to Fe^{2+} ions on the core-shell of the magnetite nanoparticles included on the composite, beside the reducing activity of some surface functional groups such as C-H or C-OH [16].

Fig. (4c) shows the FTIR spectrum of (SCB-BC/ Fe_3O_4) nano-composite after adsorption of Zn on its surface. Comparing with the FTIR spectrum of pure composite (fig. 3a) five common characteristic peaks with stable appearance can be detected, peak no (3) at 3425 cm^{-1} attributed to (O-H) groups, peak no (4) at 2925 cm^{-1} attributed to (CH-) stretching for alkyl, peak no (6) 1614 cm^{-1} attributed to (C-O) asymmetric, peak no (7) 1444 cm^{-1} attributed to (C=O) stretching vibration. The observed changes were as follow;

1- Disappearance of peak no (3) at 1696 cm^{-1} attributed to (C=O) carboxylic acid stretch from the composite spectrum (fig. 3a) suggesting a metal chelation complexation reaction of the Zn^{2+} metal ions from the standard zinc solution with the carboxylic group forming Zn-O [16]. This reaction confirmed by appearance of peak no (12) at 573 cm^{-1} related to metal-oxide bond [31] (i.e. the zinc ions adsorbed on the composite surface).

2- The peak no (9) represent small shift of alcoholic (C-O) group from 1112 cm^{-1} to 1104 cm^{-1}. This shift may refer to the reaction of the carbonyl group present on the composite surface attracting the Zn^{2+} metal ions from the standard zinc solution forming (Zn-O) by ion exchange reaction.

3- Appearance of new peaks no (8) at 1253cm^{-1} and no (10) at 1034 attributed to (OH) and (C-O) agreed with [33] FTIR spectrum of SCB-BC MB.

4- Disappearance of peaks no (9, 10) (Fe-O) of the octahedral and tetrahedral magnetite core from the composite spectrum (fig. 3a) at 464 cm^{-1} and 413 cm^{-1} also prove replacement of Fe-O by Zn-O. This replacement indicated complete adsorption of the Zn^{2+} metal ions from the standard zinc solution on the composite surface may by complexation reaction using Fe-O from the composite surface forming metal-ligand complexes (i.e H-Fe-O-Zn) or by using OH groups forming metal oxides Zn-O.

It was found that decreasing oxygen content may increase the affinity for adsorption [37], to the converse, oxygen-bearing function groups found to show adverse effect on organic compound adsorption [38].

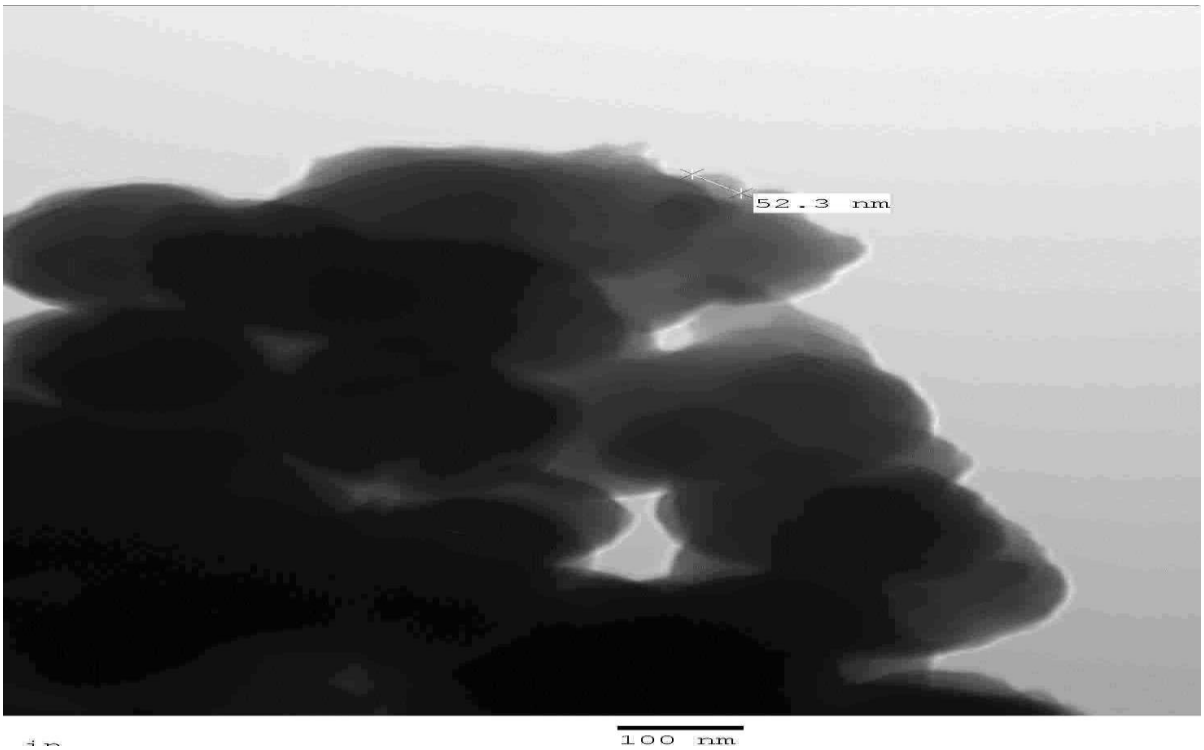

Fig. 5. Morphology of the as-prepared SCB-BC/Fe_3O_4 nano-composite, high-resolution TEM image

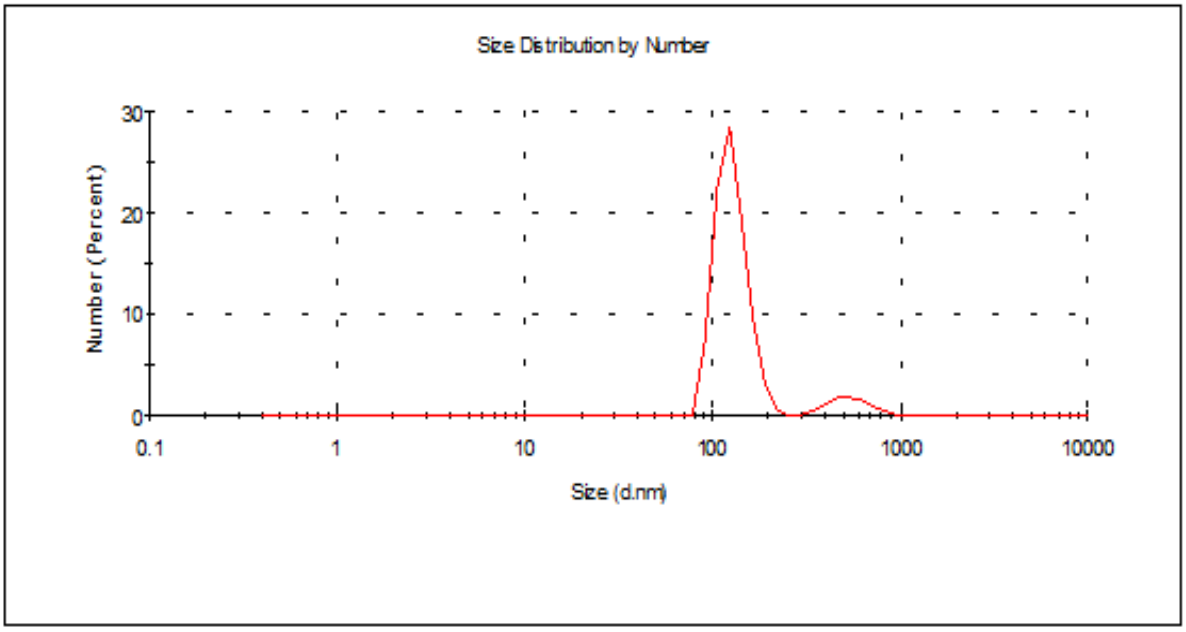

Fig. 6. Particle size distribution curve of SCB-BC

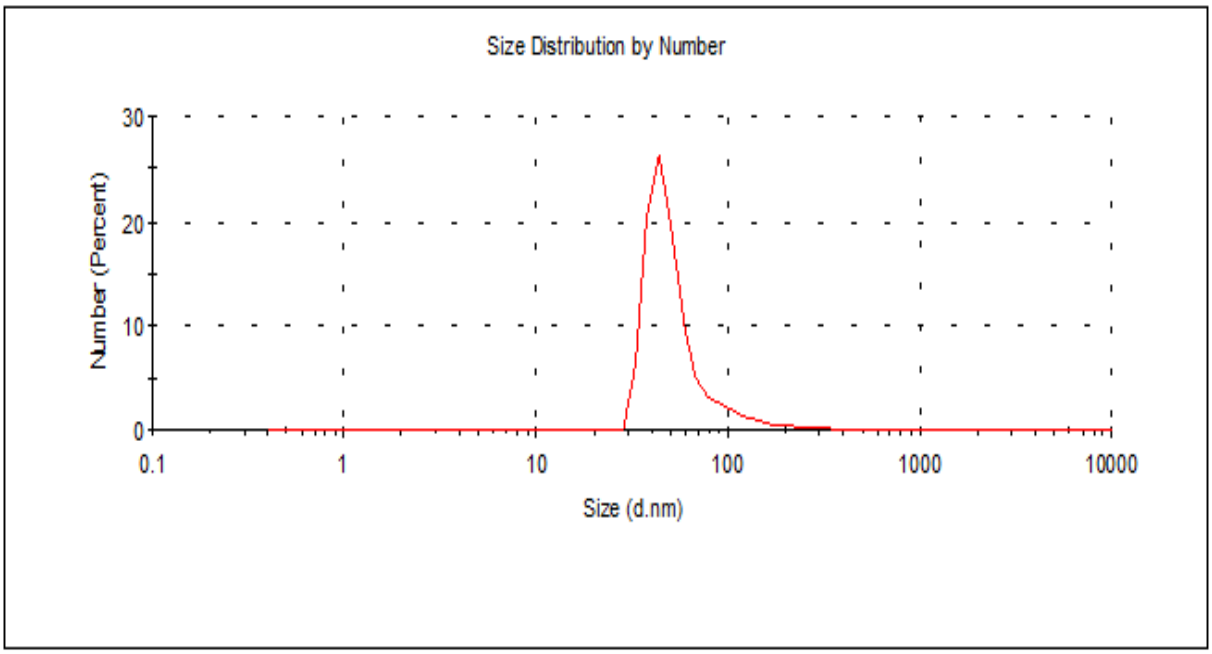

Fig. 7. Particle size distribution of curve SCB-BC/Fe_3O_4 nano-composite

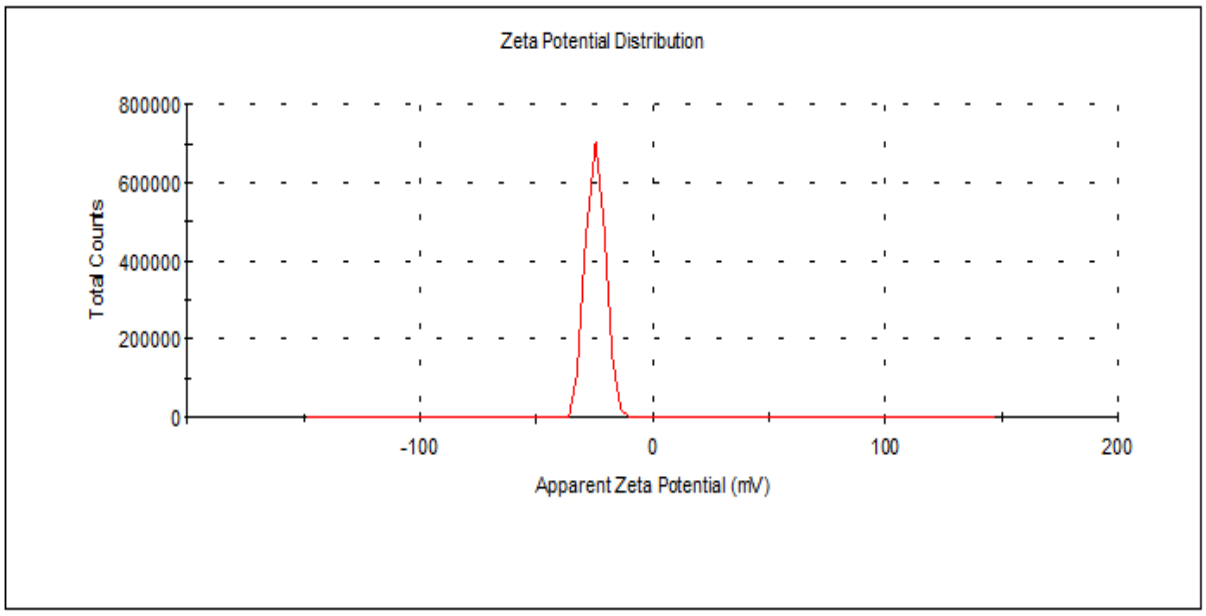

Fig. 8. The zeta potential curve of SCB-BC/Fe3O4 nano-composite

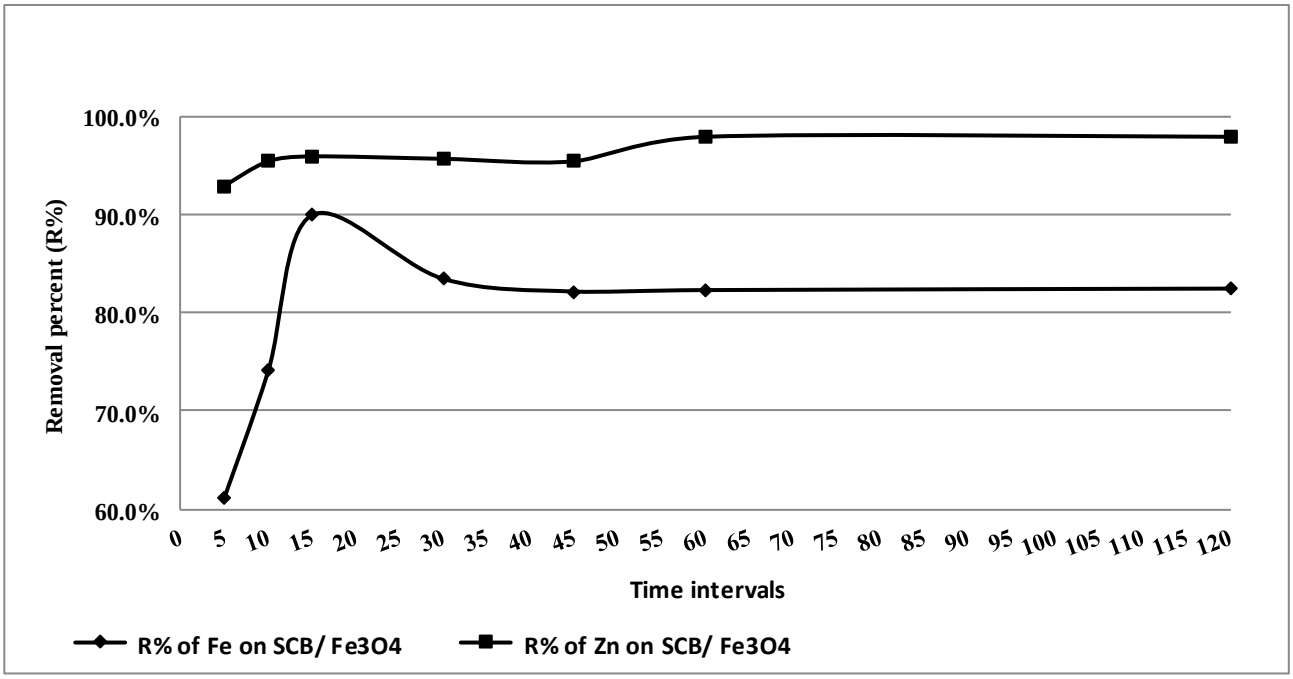

Fig. 9. Relationship between removal efficacy (R) and time intervals for adsorbed Fe and Zn (1ppm)

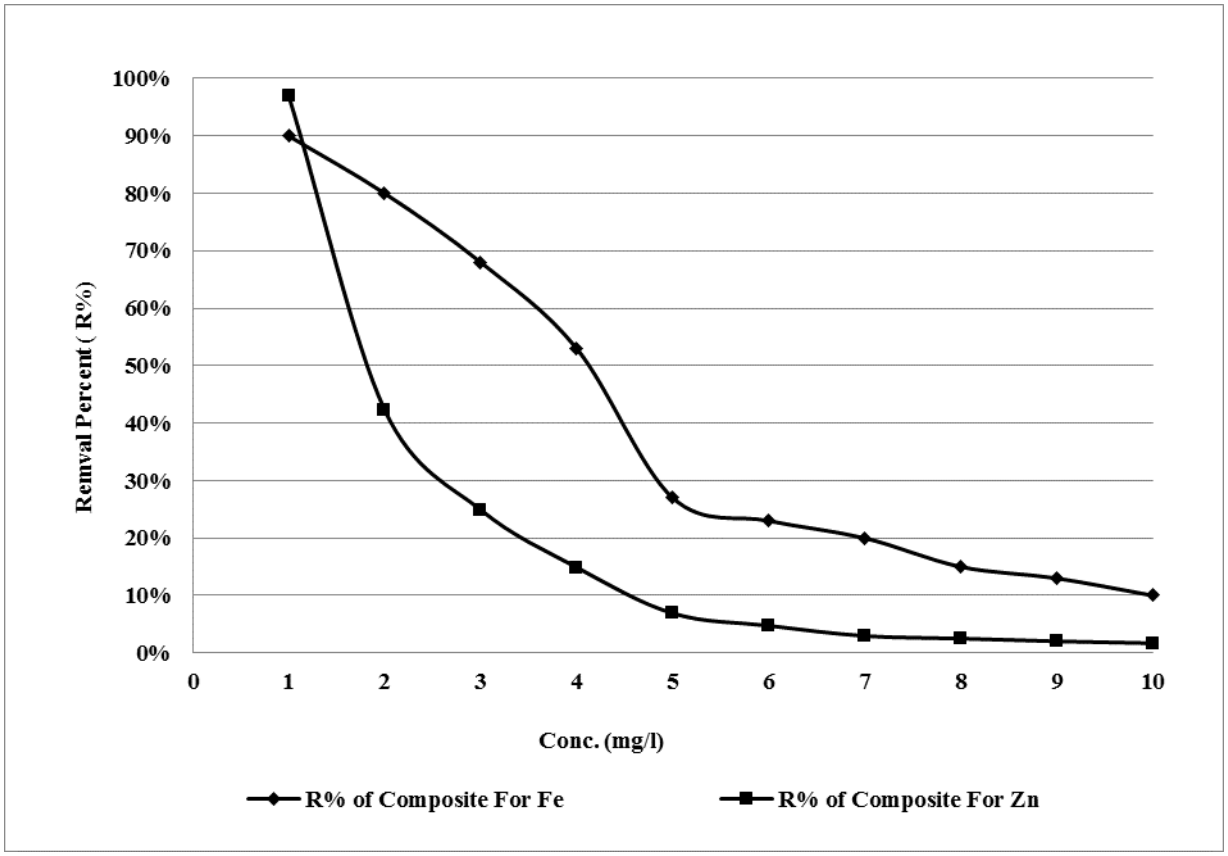

Fig. 10. Relationship between removal efficacy (R) and the initial aqueous Fe and Zn concentrations

(a)

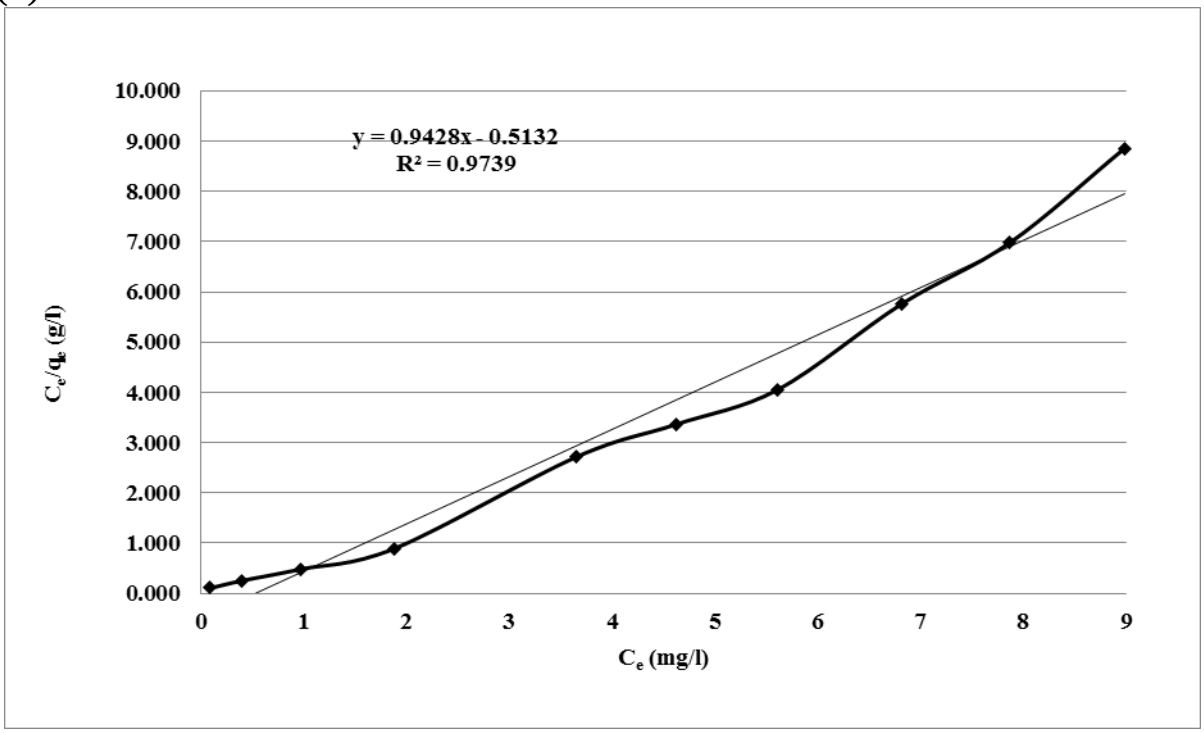

(b)

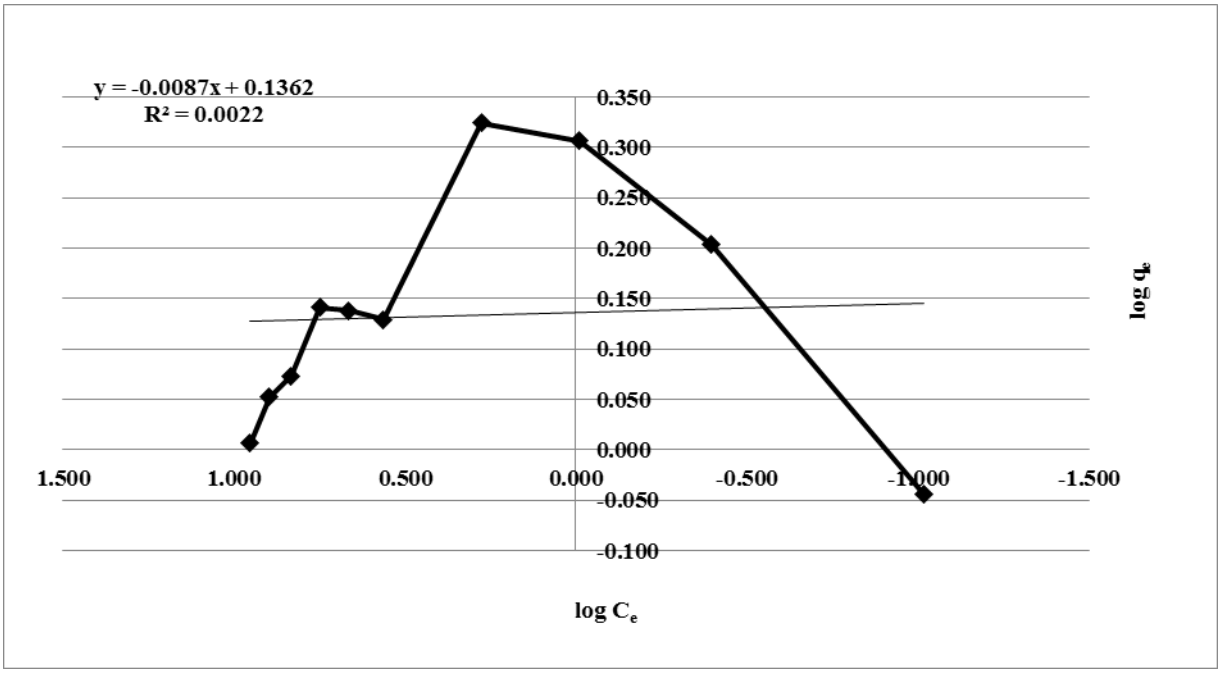

Fig. 11. Experimental data of (1ppm) Fe adsorption onto SCB/Fe_3O_4 composite fitted to linearized forms of (a) Langmuir and (b) Freundlich isotherms

(a)

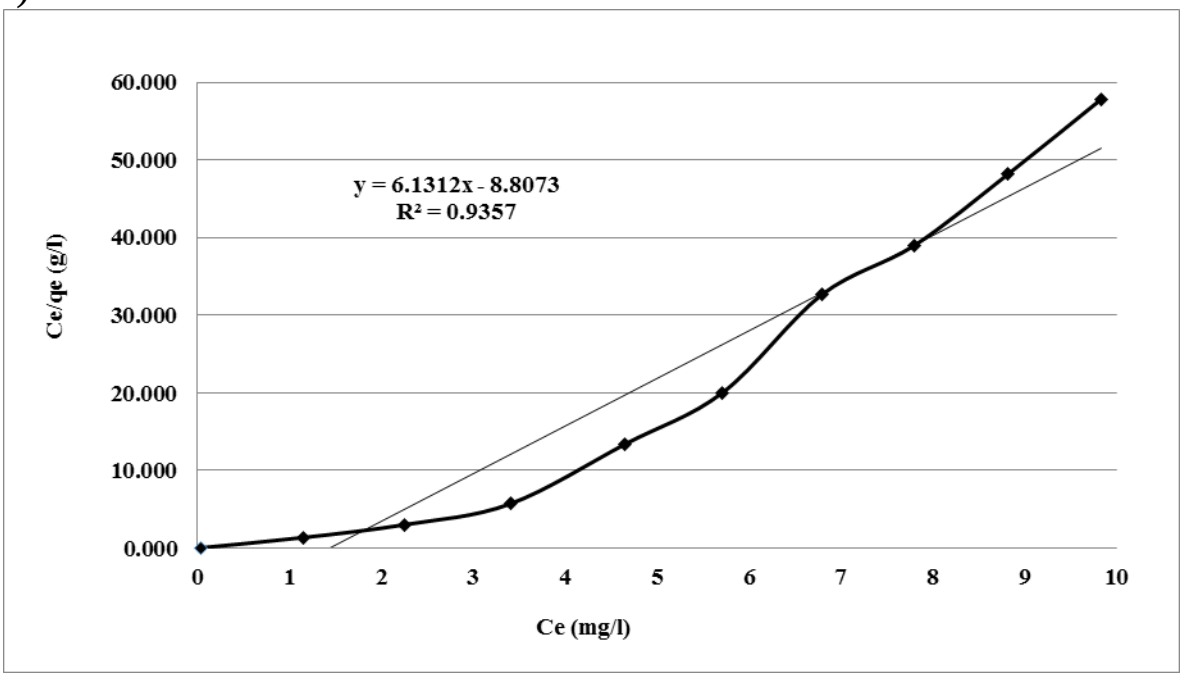

(b)

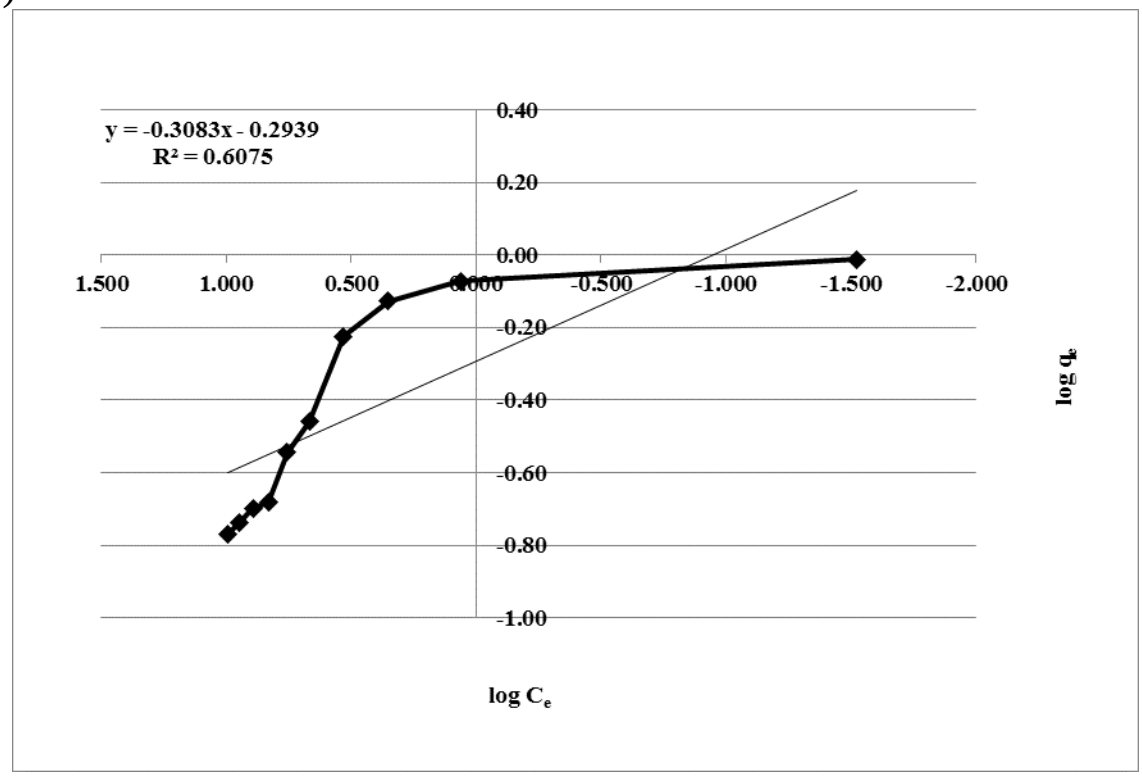

Fig. 12. Experimental data of Zn adsorption (1ppm) onto SCB/Fe_3O_4 composite fitted to linearized forms of (a) Langmuir and (b) Freundlich isotherms

3.3.2 HR-TEM analysis

HR-TEM image as shown in fig (5) used to determine the size and morphology of SCB-BC/ Fe_3O_4 nano-composite. This indicated a spherical shape and structure of the nano-particles and its size noted to be 50 nm. It was possible to observe porous structures and larger pores with some agglomerations, the observed porous structure of SCB-BC/ Fe_3O_4 nano-composite was agreed to the structure that was illustrated [29, 33].

3.3.3 DLS analysis

Fig. (6) Presents the distribution of sugarcane bagasse biochar by particle size. The average size of raw SBC-biochar particles burned at 300 °C was appeared by sharp peak at 127.5 nm. Fig. (7) Show the particle size distribution of SCB-BC/ Fe_3O_4 nano-composite, it was observed that the mean particle size of the composite was appeared by sharp peak at 57.18nm, this size confirmed the composite particle size (57.3nm) appeared in HR-TEM image fig. (5). The shift noted to smaller size of nano-particles at the particle size distribution scale proving from 127.5 nm to 57.18nm proving that the mechanical mixing of SCB-biochar with nano-magnetite reduced the particle size of SCB-biochar, i.e. SCB- BC and nano-magnetite interacted with each other and impregnated onto each other successfully forming nano-composite, and these results also agreed with the shifts noted in the FTIR spectrums of pure SCB-biochar and SCB-BC/Fe_3O_4 nano-composite.

3.3.4 Zeta potential analysis

The zeta potentials of SCB-BC/ Fe_3O_4 nano-composite are determined to be negative as shown in fig. (8) with sharp peak appeared at (-24.6mV) and the adsorbent will take up the cations with higher affinity. This result agreed with [30] who proved that SCB-biochar has net charge with negative values at different pHs, while [39] mentioned that the Fe_3O_4 nano-particles are positively charged in neutral and acidic media. The positive charge occurs as a result of proton adsorption to the neutral surface OH-groups. When pH rises, the overloading of all observed nano-magnetite particles results from the dissociation of surface OH-groups and the presence of negative charges observed by the following equation

$$Fe\text{-}OH\ (surf) + OH^- \leftrightarrow Fe\text{-}O^- + H2O \quad \rightarrow (3)$$

The negative surface charge appeared in our composite proved that nano-magnetite affected by SCB-biochar negative charge means that nano-magnetite impregnated onto SCB-biochar surface forming the composite.

3.4 The adsorption studies onto (SCB-BC/Fe_3O_4) nano-composite

3.4.1 Effect contact time on the adsorption onto the SCB-BC/Fe_3O_4 nano-composite

The relationship between the contact time and removal efficiencies of 1ppm from Fe and 1ppm Zn ions adsorbed by the SCB-BC/Fe_3O_4 nano-composite illustrated in fig. (9) and table (4), the bio-sorbent dose was 0.15g/150mL. The adsorption reached equilibrium within 15min for the initial concentrations, thereafter it became nearly constant. The percent of the metal ions removed gradually with time increases, and reached its maximum level after 15 min. This observation can be explained by increase the filling surface of the adsorbent then super-saturation takes place [34]. This affinity related to the concept that, at the beginning of the adsorption large numbers of vacated surface sites are available but after lapse time the rest vacant surface areas are difficult to be occupied. Repulsion forces between solute molecules that adsorbed on the surface of adsorbent and the bulk phase solution decreases the metal adsorption [34]. These results agreed with [24] who noted that Fe^{2+}, and Zn^{2+} ions removed by the magnetite nano-rods adsorbents during 20min with efficiencies more than 90%, this curve also agreed with [30] results for Cd^{2+} removal using the bagasse. It can be concluded that the rate of binding of Fe or Zn to the composite is higher at the initial stages, then gradually decreases and becomes almost constant after 15min.

3.3.3 Effect of the metal ion concentrations on the adsorption onto the SCB-BC /Fe_3O_4 nano-composite

Fig. (10) and table (5) Shows relationship between the removal efficiency (R) and the initial aqueous Fe and Zn concentrations. Stating from (1 to 10 ppm) for each metal ion, it was noted for Fe and Zn ions that both reached their maximum adsorption at 1ppm achieving higher removal efficiencies of 90% and 96% for Fe and Zn respectively, then further increase in the concentrations lead to an observable decrease in the removal efficiencies for the two metal ions. This may be related to the pH of the solution, as the standards of Fe and Zn are prepared in aqueous nitric acid solution so any increase in the metal ion concentration leads to more acidic solution (i.e. low pH), it is known that our composite negatively charged from the zeta potential results, so it highly attracted the positively charged Fe and Zn ions till pH 6. Below this pH value, the composite become positively charged i.e its adsorption capacity for the ions decrease. The pH_{pzc} value is the point at which functional surface groups don't add to the solution's pH. The surface charge is negative above this pH value and the adsorbent takes on cations with higher affinity [40]. As illustrated by [41, 1, 42] one of the key factors affecting pollutant adsorption of water is

the pH of the solution. With a lower pH level, it is possible to increase the removal rate of contaminants by raising the solution pH, pollutant removal rate decreased if solution pH reached the optimal value. This might to be associated with the steady saturation of the active adsorption sites, and the electrostatic repulsion between the ions [43]. These results agreed with [24] who illustrated that the initial concentrations of Fe and Zn metal ions were totally removed. On the other hand, further increase in metal ions concentrations decreases its removal efficiency. This fact can be related to that the pore sizes of the composite have been completely filled at higher concentration.

3.3.4 Adsorption isotherms

Concentrations from 1 to 10 ppm were used to assess the ability of the (SCB-BC/Fe_3O_4) nano-composite for adsorption against the examined metal ions. Using adsorption isotherms, the overall adsorption ability of the (SCB-BC/ Fe_3O_4) nano-composite adsorbent to metal ions was assessed. The isothermic models Langmuir and Freundlich were used for isotherm adsorption. The Langmuir adsorption model, assumes that all the sites of adsorption on the adsorbent surface have an equal binding capacity, and each site attach just one adsorbent. ***The linearized Langmuir isotherm*** is given as following equation

$$C_e/q_e = (1/bq_m) + (C_e/q_m) \quad \rightarrow (4)$$

where;

q_e is the equilibrium adsorbent ability removing metal ion concentrations in mg/g.

C_e is the metal ions concentration in equilibrium by mg/l.

q_m is the highest limit of the adsorbed metal ions in mg/g and b the constant referring to the bonding energy is of sorption process.

The b (L/mg) and q_m constants can be determined from the intercept and slope of C_e/q_e against C linear diagram [24].

The equilibrium adsorbent ability q_e can be calculated by equation

$$q_e = (C_i\text{-}C_e) *V/m \quad \rightarrow (5)$$

where;

C_i (mg/l) and C_e (mg/l) are the initial and equilibrium concentrations of the metal ions (Fe and Zn).

V (ml) is the adsorbate (standard Fe or Zn solution) volume (150ml).

m (mg) is the adsorbent (SCB-BC/ Fe_3O_4) nano-composite weight (0.15g = 150mg) [24].

The favorable adsorption character may be expressed in terms of dimensionless parameter called separation factor, which is specified

$$R_L = 1/ (1+bC_0) \quad \rightarrow (6)$$

where;

C_0 (mg/l) is the initial concentration of the adsorbate (standard Fe or Zn solution)

b (l/mg) is the Langmuir constant

The R_L value states the Langmuir model type indicating the nature of the metal ions adsorption on the composite

(R_L = 0 irreversible), (0 < R_L < 1 favorable), (R_L = 1 linear) or (R_L > 1 unfavorable) [44].

On the opposite side, the Freundlich model is based on reversible heterogeneous adsorption heterogeneity of the adsorption sites binding energy.

The linear equation of the Freundlich isotherm is given as:

$$\log q_e = \log K_f + (1/n) \log C_e \quad \rightarrow (7)$$

where;

q_e is the adsorbent ability removing metal ion concentrations in mg/g.

C_e is the metal ions concentration in equilibrium by mg/l.

K_f is the adsorption efficiency of the adsorbent constant in mg/l, and n is the adsorption strength constant.

The n and K_f constants can be determined from the slope and intercept of the log q_e versus log C_e linear diagram determined from the intercept and slope of the linear plot C_e/q_e versus C [24].

The adsorption isotherms for both Fe and Zn were shown in figs. (11,12). The calculated (q_m and b) values for the Langmuir model, the calculated (n and K) for the Freundlich model, separation factor (R_L) and linear regression coefficient (r^2) values are given in table (6). The results showed that the Langmuir correlation coefficient values (r^2) for Fe and Zn adsorption onto (SCB-BC/Fe_3O_4) nano-composite were 0.9739 and 0.9357 respectively, while the Freundlich correlation coefficient values (r^2) for Fe and Zn adsorption onto (SCB-BC/Fe_3O_4) nano-composite were 0.0022 and 0.6075 respectively, proving that experimental data good fited to the Langmuir model's verifying the monolayer applicability. These results agreed with [24] who illustrated that the removal of all Fe and Zn metal ions onto magnetite nanorods as an adsorbent was better to fit the Langmuir isotherm with the experimental data than Freundlich model. The R_L values for both Fe and Zn over the working concentration range (1-10 mg/l) showed separation factor greater than zero and less than 1 (0 < R_L < 1) reporting favorable adsorption. The heavy metals were adsorbed after being coated by the composite. Adsorption energy is not identical in Freundlich model as its affinity towards the adsorbent are not the same [45].

Numerous studies examined the viability of using different sorbents, the gained data showed that the adsorption capacity of the magnetite nanoparticles (3.7mg g^{-1}) [46], magnetic nanoparticle (γ-Fe_2O_3)-coated zeolite (MNCZ) (19.39mg g^{-1}) [47], biochar (1.998 mg g^{-1}) [37] and activated carbon (42.3 and 20.2 mg g^{-1}) [48]. The adsorption capacities of $Fe^{2+}$and Zn^{2+} by magnetite nanorods based on the Langmuir model, were 127 and 107 mg g^{-1}, respectively illustrated by [24]. These capacities were determined for single-solute system. However in our study The adsorption capacities of $Fe^{2+}$and Zn^{2+} by (SCB-BC/Fe_3O_4) nano-composite based also on the Langmuir model, were 1.06 and 0.163 mg g^{-1}, respectively table (6).

3.3.5 Application of the SCB-BC/ Fe_3O_4 nanocomposite to domestic wastewater

The results showed that 0.15 g of the prepared SCB-BC/ Fe_3O_4 nanocomposite can remove nitrate, total phosphorous (TP), COD, BOD, total coliform and fecal coliform concentrations approximately to 33%, 86%, 83%, 88%, 100% respectively table (7). The removal efficiency of our composite for COD and BOD completely agreed with [45] who used Fe_3O_4/Bentonite magnetic composite for removing the same pollutants from industrial wastewater coming from a pharmacy unit. This comparison prove that using of composites containing Fe_3O_4 achieve good results in pollutants removal. Comparing our obtained data with other authors used different adsorbents to remove COD and BOD from wastewater, we obtained data displayed that COD and BOD removed by percentage 95.4% and 92.8% respectively by activated carbon dosage of 0.1 g/100 ml of solution, and the adsorption equilibrium was achieved after 150 min at pH 6.0 with agitation rate of 400 rpm at 25 °C [48]. However in this study, COD and BOD removed by percentage 83% and 88% respectively from 150 ml real wastewater sample collected from the final effluent of domestic wastewater by 0.15 g of SCB-BC/Fe_3O_4 nano-composite and the adsorption equilibrium was attained after 15 min at pH 7.0 with agitation rate of 200 rpm. The same comparisons were done for heavy metals, the obtained data showed cadmium ions removal reached 98.88% by ceramic nano-particles using Ceramic/CuO nano-composite [49]. However in this study, iron ions removed by 89% percentage and zinc ions removed by 93.4% percentage using SCB-BC/Fe_3O_4 nano-composite.

Table 6: Langmuir and Freundlich isotherm parameters for Fe and Zn adsorption on SCB-BC/Fe_3O_4 nanocomposite

Adsorption isotherm	Parameter	Value	
		Fe	Zn
Langmuir	q_m	1.06	0.163
	B	0.544	1.44
	r^2	0.9739	0.9357
	R_L calculated using C_0 = 1mg/l	0.65	0.41
Freundlich			
	K	1.37	2
	n	114.9	3.24
	R^2	0.0022	0.6075

Table 7: SCB-BC/Fe_3O_4 nanocomposite performance in removing nitrate, T, BOD, COD, total , fecal coliforms , iorn and zinc from real samples of domestic wastewater

Pollution index	Intial values	final values	Removal%
NO_3	1.995 ppm	1.33 ppm	33.30%
TP	Abs. 0.051	Abs. 0.007	86%
BOD	8.5 ppm	1 ppm	88%
COD	60 ppm	10 ppm	83%
T. Coli	16000 MPN/100ml	Nil	100%
F.Coli	Nil	Nil	100%
PH	7.82	8.19	
Fe	4.641 ppm	0.517 ppm	89%
Zn	0.124 ppm	0.0082 ppm	93.40%
$R.Cl_2$	0.46		

4. Conclusions

- Pyrolysis temperature influences the physical and chemical properties of the biochar, thereby influencing its pollutant removal efficiency.
- The concentration ratio of biochar and Fe_3O_4 affects the removal efficiency of metals.
- The mechanical mixing of SCB-biochar with nano-magnetite to form nano-composite is successful novel mechanism, characterization data showed that each material could affect each other, the changes noted in the FTIR spectrums and DLS cruves of SCB-biochar and SCB-BC/ Fe_3O_4 nano-composite.
- Changes of the particle size distribution curve of SCB-biochar from 127.5 nm to 57.3 nm in the composite and the surface charge of nano-magnetite that affected by negative charge of biochar resulting in net negative charge of composite, confirmed that the mechanical mixing affected the both size and charge.
- Removal of the contaminants increased by the start of the reaction, then decreased gradually as natural result of receptive points of biochar being saturated by the adsorbed metals.

5.Conflicts of interest

We are the authors of this manuscript disclose any potential sources of conflict of interest. Any interest or relationship, financial or otherwise that might be perceived as influencing our objectivity was totally avoided

6.Acknowledgments

The authors would like to express great thankful for Environmental Research Department, Land, Water and Environment Institute, Agricultural Research Center, Ministry of Agriculture for hosting this work and providing support for the authors.

6.References

[1] Zhang, Y., Wu, B., Xu, H., Liu, H., Wang, M., He, Y., & Pan, B. **2016**. Nanomaterials-enabled water and wastewater treatment. *NanoImpact*, *3*, 22-39. 2.

[2] Järup, L. **2003**. Hazards of heavy metal contamination. *British medical bulletin*, *68*(1), 167-182. (CF Li, H., Dong, X., da Silva, E. B., de Oliveira, L. M., Chen, Y., & Ma, L. Q. **2017**. Mechanisms of metal sorption by biochars: biochar characteristics and modifications. *Chemosphere*, *178*, 466-478.

[3] Li, H., Dong, X., da Silva, E. B., de Oliveira, L. M., Chen, Y., & Ma, L. Q. **2017**. Mechanisms of metal sorption by biochars: biochar characteristics and modifications. *Chemosphere*, *178*, 466-478.

[4] Vaaramaa, K., & Lehto, J. **2003**. Removal of metals and anions from drinking water by ion exchange. *Desalination*, *155*(2), 157-170. (CF Nagappan, S., Ha, H. M., Park, S. S., Jo, N. J., & Ha, C. S. (2017). One-pot synthesis of multi-functional magnetite polysilsesquioxane hybrid nanoparticles for the selective Fe^{3+} and some heavy metal ions adsorption. *RSC advances*, *7*(31), 19106-19116.

[5] Chaturvedi, S., & Dave, P. N. **2012**. Removal of iron for safe drinking water. *Desalination*, *303*, 1-11.

[6] Nagappan, S., Ha, H. M., Park, S. S., Jo, N. J., & Ha, C. S. **2017**. One-pot synthesis of multi-functional magnetite polysilsesquioxane hybrid nanoparticles for the selective Fe^{3+} and some heavy metal ions adsorption. *RSC advances*, *7*(31), 19106-19116.

[7] Ahmed, M. B., Zhou, J. L., Ngo, H. H., Guo, W., Johir, M. A. H., & Belhaj, D. **2017**. Competitive sorption affinity of sulfonamides and chloramphenicol antibiotics toward functionalized biochar for water and wastewater treatment. *Bioresource technology*, *238*, 306-312.

[8] Rosales, E., Meijide, J., Pazos, M., & Sanromán, M. A. **2017**. Challenges and recent advances in biochar as low-cost biosorbent: from batch assays to continuous-flow systems. *Bioresource technology*, *246*, 176-192.

[9] Li, J., Zheng, L., Wang, S. L., Wu, Z., Wu, W., Niazi, N. K et al., & Wang, H. **2019d**. Sorption mechanisms of lead on silicon-rich biochar in aqueous solution: Spectroscopic investigation. *Science of the Total Environment*, *672*, 572-582.

[10] Li, L., Zou, D., Xiao, Z., Zeng, X., Zhang, L., Jiang, L et al., & Liu, F. **2019**. Biochar as a sorbent for emerging contaminants enables improvements in waste management and sustainable resource use. *Journal of cleaner production*, *210*, 1324-1342.

[11] Mashego, D. V. **2016**. Preparation, isolation and characterization of nanocellulose from sugarcane bagasse *(Doctoral dissertation)*.

[12] Corr, S.A. **2013**. Metal oxide nanoparticles. *Nanoscience*, *1*, 180–234.

[13] Laurent, S., Forge, D., Port, M., Roch, A., Robic, C., Vander Elst, L., & Muller, R. N. **2008**. Magnetic iron oxide nanoparticles: synthesis, stabilization, vectorization, physicochemical characterizations, and biological applications. *Chemical reviews*, *108*(6), 2064-2110.

[14] Qu, X., Alvarez, P. J., & Li, Q. **2013**. Applications of nanotechnology in water and wastewater treatment. *Water research*, *47*(12), 3931-3946.

[15] Predescu, A., Matei, E., Predescu, A., DASCĂLU, O., & Predescu, C. **2015**. EFFICIENT METHODS FOR NANOMAGNETITE SYNTHESIS. *UPB SciBull. Ser. B*, *74*, 1454-2331.

[16] Ho, S. H., Zhu, S., & Chang, J. S. **2017**. Recent advances in nanoscale-metal assisted biochar derived from waste biomass used for heavy metals removal. *Bioresource technology*, *246*, 123-134.

[17] Li, H., Xiong, J., Zhang, G., Liang, A., Long, J., Xiao, T., & Zhang, H. **2020**. Enhanced thallium (I) removal from wastewater using hypochlorite oxidation coupled with magnetite-based biochar adsorption. *Science of the Total Environment*, *698*, 134166.

[18] APHA, 2005. In: Standard Methods for the Examination of Water and Wastewater, 20th ed. American Public Health Association, Washington, DC, USA. ICP measurements method, 3120B.

[19] Zayed, M. A., Ahmed, M. A., Imam, N. G., & El Sherbiny, D. H. **2016**. Preparation and structure characterization of hematite/magnetite ferro-fluid nanocomposites for hyperthermia purposes. *Journal of Molecular Liquids*, *222*, 895-905.

[20] Agrafioti, E., Kalderis, D., & Diamadopoulos, E. **2014**. Ca and Fe modified biochars as adsorbents of arsenic and chromium in aqueous solutions. *Journal of environmental management*, *146*, 444-450.

[21] Yaashikaa, P. R., Kumar, P. S., Varjani, S. J., & Saravanan, A. **2019**. Advances in production and application of biochar from lignocellulosic feedstocks for remediation of environmental pollutants. *Bioresource technology*, 122030.

[22] Han, Z., Sani, B., Mrozik, W., Obst, M., Beckingham, B., Karapanagioti, H. K., & Werner, D. **2015b**. Magnetite impregnation effects on the sorbent properties of activated carbons and biochars. *Water research*, *70*, 394-403.

[23] Li, Y., Cheng, W., Sheng, G., Li, J., Dong, H., Chen, Y., & Zhu, L. **2015**. Synergetic effect of a pillared bentonite support on SE (VI) removal by nanoscale zero valent iron. *Applied Catalysis B: Environmental*, *174*, 329-335.

[24] Karami, H. **2013**. Heavy metal removal from water by magnetite nanorods. *Chemical Engineering Journal*, *219*, 209-216.

[25] Argun, M. E., Dursun, S., & Karatas, M. **2009**. Removal of Cd (II), Pb (II), Cu (II) and Ni (II) from water using modified pine bark. *Desalination*, *249*(2), 519-527.

[26] Reddy, D. H. K., & Lee, S. M. **2014**. Magnetic biochar composite: facile synthesis, characterization, and application for heavy metal removal. *Colloids and Surfaces A: Physicochemical and Engineering Aspects*, *454*, 96-103.

[27] Saleh, S., Kamarudin, K. B., Ghani, W. A. W. A. K., & Kheang, L. S. **2016**. Removal of organic contaminant from aqueous solution using magnetic biochar. In *4th International Conference on Process Engineering and Advanced Materials* (Vol. 148, pp. 228-235).

[28] Wang, P., Tang, L., Wei, X., Zeng, G., Zhou, Y., Deng, Y., & Fang, W. **2017**. Synthesis and application of iron and zinc doped biochar for removal of p-nitrophenol in wastewater and assessment of the influence of co-existed Pb (II). *Applied Surface Science*, *392*, 391-401.

[29] Adinaveen, T., Kenndy, L. J., Vijaya, J. J., & Sekaran, G. **2013**. Studies on structural, morphological, electrical and electrochemical properties of activated carbon prepared from sugarcane bagasse. *Journal of industrial and Engineering Chemistry*, *19*(5), 1470-1476.

[30] Moubarik, A., & Grimi, N. **2015**. Valorization of olive stone and sugar cane bagasse by-products as biosorbents for the removal of cadmium from aqueous solution. *Food Research International*, *73*, 169-175.

[31] Buthiyappan, A., Gopalan, J., & Raman, A. A. A. **2019**. Synthesis of iron oxides impregnated green adsorbent from sugarcane bagasse: Characterization and evaluation of adsorption efficiency. *Journal of environmental management*, *249*, 109323.

[32] Devi, P., & Saroha, A. K. **2014**. Synthesis of the magnetic biochar composites for use as an adsorbent for the removal of pentachlorophenol from the effluent. *Bioresource technology*, *169*, 525-531.

[33] Noraini, M. N., Abdullah, E. C., Othman, R., & Mubarak, N. M. **2016**. Single-route synthesis of magnetic biochar from sugarcane bagasse by microwave-assisted pyrolysis. *Materials Letters*, *184*, 315-319.

[34] Ahmad, I., Siddiqui, W. A., & Ahmad, T. **2019**. Synthesis and characterization of molecularly imprinted magnetite nanomaterials as a novel adsorbent for the removal of heavy metals from aqueous solution. *Journal of Materials Research and Technology*, *8*(5), 4239-4252.

[35] Tong, M., He, L., Rong, H., Li, M., & Kim, H. **2020**. Transport behaviors of plastic particles in saturated quartz sand without and with biochar/Fe_3O_4-biochar amendment. *Water research*, *169*, 115284.

[36] Utkan, G. G., Sayar, F., Batat, P., Ide, S., Kriechbaum, M., & Pişkin, E. **2011**. Synthesis

and characterization of nanomagnetite particles and their polymer coated forms. *Journal of colloid and interface science*, *353*(2), 372-379.

[37] Taheran, M., Naghdi, M., Brar, S. K., Knystautas, E. J., Verma, M., Ramirez, A. A., & Valéro, J. R. **2016**. Adsorption study of environmentally relevant concentrations of chlortetracycline on pinewood biochar. *Science of the Total Environment*, *571*, 772-777.

[38] Derylo-Marczewska, A., Buczek, B., & Swiatkowski, A. **2011**. Effect of oxygen surface groups on adsorption of benzene derivatives from aqueous solutions onto active carbon samples. *Applied surface science*, *257*(22), 9466-9472.

[39] Manilo, M. V., Netreba, S. V., Prokopenko, V. A., Lebovka, N. I., & Barany, S. **2016**. Overcharging of magnetite nanoparticles in electrolyte solutions. *Colloids and Surfaces A: Physicochemical and Engineering Aspects*, *506*, 291-297.

[40] Marcilla, A., Beltrán, M. I., & Navarro, R. **2007**. Application of TG/FTIR to the study of the regeneration process of husy and HZSM5 zeolites. *Journal of thermal analysis and calorimetry*, *87*(2), 325-330.

[41] Kołodyńska, D., Wnętrzak, R., Leahy, J. J., Hayes, M. H. B., Kwapiński, W., & Hubicki, Z. J. C. E. J. **2012**. Kinetic and adsorptive characterization of biochar in metal ions removal. *Chemical Engineering Journal*, *197*, 295-305.

[42] Ifthikar, J., Wang, J., Wang, Q., Wang, T., Wang, H., Khan, A., & Chen, Z. **2017**. Highly efficient lead distribution by magnetic sewage sludge biochar: sorption mechanisms and bench applications. *Bioresource technology*, *238*, 399-406.

[43] Li, X., Wang, C., Zhang, J., Liu, J., Liu, B., & Chen, G. **2020**. Preparation and application of magnetic biochar in water treatment: A critical review. *Science of The Total Environment*, *711*, 134847.

[44] Roy, A., & Bhattacharya, J. **2012**. Removal of Cu (II), Zn (II) and Pb (II) from water using microwave-assisted synthesized maghemite nanotubes. *Chemical Engineering Journal*, *211*, 493-500.

[45] Khatamian, M., Divband, B., & Shahi, R. **2019**. Ultrasound assisted co-precipitation synthesis of Fe3O4/bentonite nanocomposite: Performance for nitrate, BOD and COD water treatment. *Journal of Water Process Engineering*, *31*, 100870.

[46] Chowdhury, S. R., & Yanful, E. K. (2011). Arsenic removal from aqueous solutions by adsorption on magnetite nanoparticles. *Water and Environment Journal*, *25*(3), 429-437.

[47] Salem Attia, T. M., Hu, X. L., & Yin, D. Q. (2014). Synthesised magnetic nanoparticles coated zeolite (MNCZ) for the removal of arsenic (As) from aqueous solution. *Journal of Experimental Nanoscience*, *9*(6), 551-560.

[48] Nayl, A., Elkhashab, R., Malah, T., Yakout, S., El-Khateeb, M., Ali, M., & Ali, H. (2017). Adsorption studies on the removal of COD and BOD from treated sewage using activated carbon prepared from date palm waste. *Environmental Science & Pollution Research*, *24*(28).

[49] Ammar, N., Fahmy, A., Kanawy Ibrahim, S., Hamzawy, E. M. A., & El-Khateeb, M. (2017). Wollastonite ceramic/CuO nano-Composite For cadmium ions removal from waste water. *Egyptian Journal of Chemistry*, *60*(5), 817-823.